



Research paper

Vinylphosphonate-based cyclic dinucleotides enhance STING-mediated cancer immunotherapy

Milan Dejmek^{a,1}, Andrea Brazdova^{a,b,1}, Tomáš Otava^{a,c}, Marketa Pimkova Polidarova^{a,b}, Martin Klíma^a, Miroslav Smola^a, Zdenek Vavrina^{a,d}, Miloš Buděšinský^a, Martin Dračínský^a, Radek Liboska^a, Evzen Boura^a, Gabriel Birkuš^{a,**}, Radim Nencka^{a,*}

^a Institute of Organic Chemistry and Biochemistry of the Czech Academy of Sciences, Flemingovo náměstí 2, Prague 6, 166 10, Czech Republic

^b Department of Genetics and Microbiology, Faculty of Science, Charles University, Prámyslová 595, Vestec, 128 44, Prague, Czech Republic

^c Faculty of Food and Biochemical Technology, University of Chemistry and Technology, 166 28, Prague 6, Czech Republic

^d Faculty of Science, Charles University, Albertov 6, Prague 2, 128 00, Czech Republic



ARTICLE INFO

Keywords:

Cyclic dinucleotides
STING
Cancer
Intratumoral administration
Immunotherapy

ABSTRACT

Cyclic dinucleotides (CDNs) trigger the cyclic GMP-AMP synthase-stimulator of interferon genes (cGAS-STING) pathway, which plays a key role in cytosolic DNA sensing and thus in immunomodulation against infections, cell damage and cancer. However, cancer immunotherapy trials with CDNs have shown immune activation, but not complete tumor regression. Nevertheless, we designed a novel class of CDNs containing vinylphosphonate based on a STING-affinity screening assay. *In vitro*, acyloxymethyl phosphate/phosphonate prodrugs of these vinylphosphonate CDNs were up to 1000-fold more potent than the clinical candidate ADU-S100. *In vivo*, the lead prodrug induced tumor-specific T cell priming and facilitated tumor regression in the 4T1 syngeneic mouse model of breast cancer. Moreover, we solved the crystal structure of this ligand bound to the STING protein. Therefore, our findings not only validate the therapeutic potential of vinylphosphonate CDNs but also open up opportunities for drug development in cancer immunotherapy bridging innate and adaptive immunity.

1. Introduction

Cancer is a major public health problem and a leading cause of mortality worldwide, accounting for 10 million deaths in 2020. The incidence of breast, colon, esophagus, kidney, liver, and pancreatic cancers, among others, has increased around the world over the last decade [1,2]. But an auspicious alternative to common cancer treatments, i.e., surgery, chemotherapy, and radiation or hormonal therapy, has been emerging in recent years. This approach consists of targeted immunomodulation whereby the host immune system is activated to target cancer cells [3].

Antibody-associated immunotherapy based on immune-checkpoint blockade (ICB) initially targeted molecules that affect T cell function, such as cytotoxic T-lymphocyte antigen 4 (CTLA-4) and programmed cell death protein 1 (PD-1). However, many tumors were found to be resistant to ICB [4–7]. For this reason, immunotherapy strategies have

more recently aimed at turning these ‘cold tumors’ into ‘hot tumors’ by improving their immunogenicity. Direct immunomodulation of specific immune subsets combined with tumor cell stimulation is a particularly promising modality of tertiary care for terminally ill cancer patients [6, 8,9]. In this context, the cyclic guanosine monophosphate-adenosine monophosphate synthase (cGAS)- Stimulator of Interferon Genes (STING) signal pathway is an excellent pharmaceutical target for its key role in both bridging innate and adaptive immune responses and inducing host anti-tumor immune responses [10,11].

cGAS is a sensor enzyme that recognizes cytoplasmic self or pathogen DNA. After binding to DNA, cGAS catalyzes the synthesis of a cyclic dinucleotide (CDN) 2',3'-cGAMP 1, which acts as a second messenger for STING [12]. STING activation enhances cancer antigen presentation, contributing to priming of tumor-specific cytotoxic CD8⁺ T cells and to trafficking and further infiltration of T cells into tumors (Figure 1) [13, 14]. Both systemic (intravenous, IV) and localized (intratumoral, IT)

* Corresponding author.

** Corresponding author.

E-mail addresses: gabriel.birkus@uochb.cas.cz (G. Birkuš), radim.nencka@uochb.cas.cz (R. Nencka).

¹ M.D. and A.B. contributed equally.

<https://doi.org/10.1016/j.ejmech.2023.115685>

Received 13 June 2023; Received in revised form 24 July 2023; Accepted 25 July 2023

Available online 26 July 2023

0223-5234/© 2023 The Authors.

Published by Elsevier Masson SAS. This is an open access article under the CC BY license (<http://creativecommons.org/licenses/by/4.0/>).

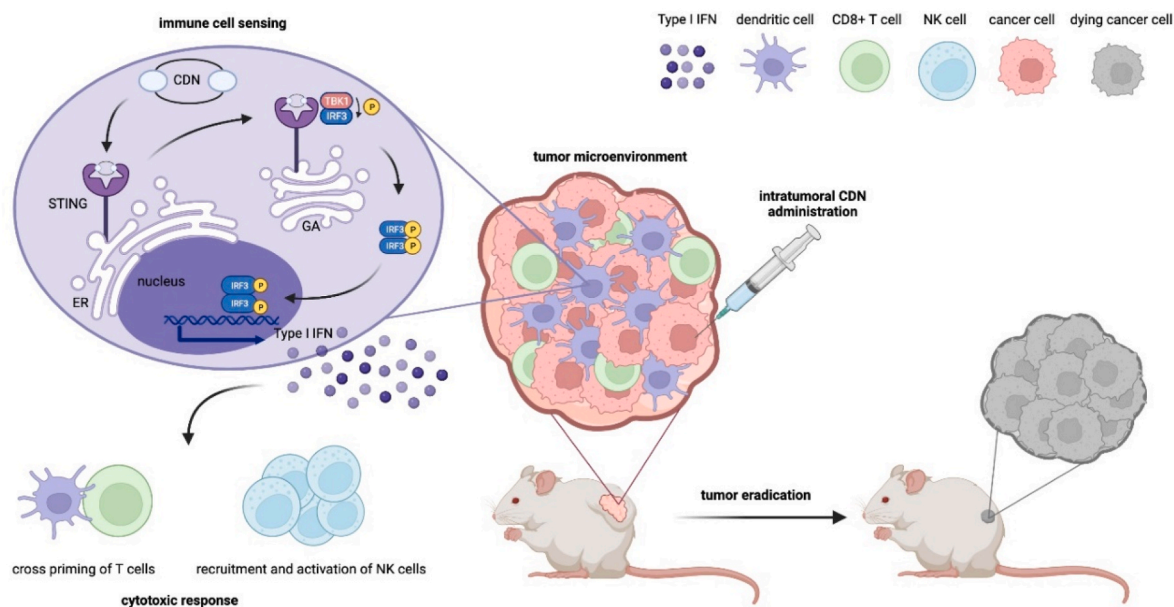


Figure 1. STING agonist-based strategy in anticancer therapy. IT STING agonist administration activates immune system factors within the tumor microenvironment by sensing the cGAS-STING pathway, leading to downstream signaling based on TBK1 and IRF3. The resulting type I interferon-driven immune response facilitates adaptive immunity, further eradicating tumor cells. CDN: cyclic dinucleotides, ER: endoplasmic reticulum, GA: Golgi apparatus, IFN: interferons, IRF3: interferon regulatory factor 3, NK: natural killer cell, STING: stimulator of interferon genes, TBK1: TANK-binding kinase 1, P: phosphorylation. Figure adapted [24–26] and modified with [BioRender.com](#).

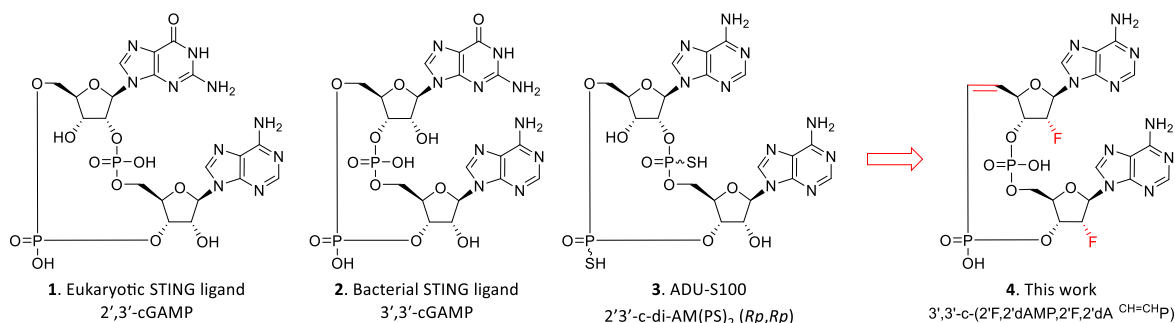
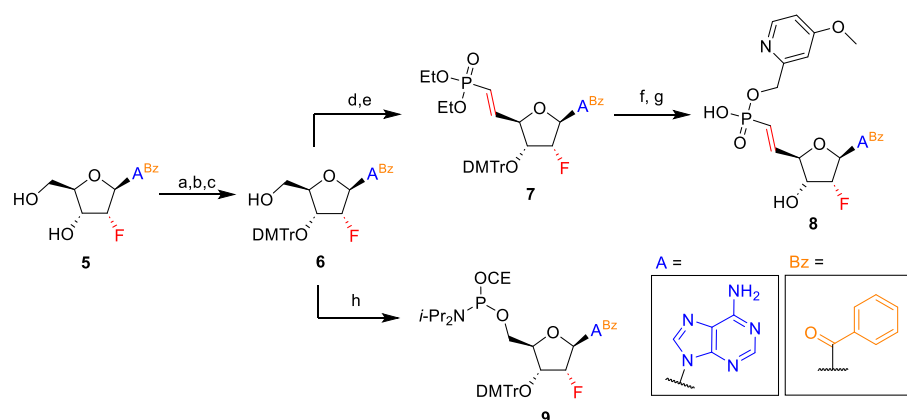


Fig. 2. Examples of naturally occurring and synthetic CDNs acting as STING agonists and the proposed vinylphosphonate-based CDN explored in this study.

application of STING agonists can lead to tumor regression in mouse models and induce specific adaptive antitumoral immunity [15]. Moreover, STING can be directly activated by various agonists (Fig. 2), including canonical (e.g., eukaryotic 2',3'-cGAMP 1, bacterial 3',3'-cGAMP 2) [16–18] and synthetic (e.g., ADU-S100 3, 3',3'-c-(2'F,

2'dAMP, ^{isonuc}AMP)) [19–21] CDNs, in addition to non-CDN small molecules (e.g., diABZI or DMXAA) [22,23]. Accordingly, considerable research efforts have been made to develop CDNs as anticancer therapeutics.

Among the CDNs that have been at the forefront of research on



Scheme 1. Synthesis of the key vinylphosphonate monomer and its complementary phosphoramidite.^a

^aReagents and conditions: a) TBDMSCl, py, r. t., 17 h; b) DMTrCl, py, 60 °C, 24 h; c) TBAF, THF, r. t., 24 h, 75% over 3 steps; d) EDCI, DMSO, TFA, py, DMF, r. t. 2h; e) tetraethyl methylenediphosphonate, *n*BuLi, THF, −78 °C, 15 min, 55% over 2 steps; f) TMSBr, py, r. t., 12 h; g) (4-methoxy-pyridin-2-yl)-methanol, DMOCp, py, r. t., 1 h then H₂O, 70 °C, 48 h, 60% over 2 steps; h) (iPr₂N)₂P-OCE, tetrazole, MeCN, r. t., 2 h, 88%.

immunomodulators, 2',3'-c-di-AM(PS)2 (*Rp,Rp*) (ADU-S100 **3**) stood out in clinical trials in patients with advanced/metastatic solid tumors or lymphomas [27], followed by MK-1454 [28] and E7766 [29]. Increased levels of inflammatory cytokines were observed in the clinical trial of ADU-S100 and MK-1454, suggesting immune activation. However, the primary goal of tumor eradication was not achieved when using these first-generation CDNs [30]. Therefore, new STING agonists must be developed to improve their potency.

Here, we present the development, optimization and characterization of a novel type of CDNs in which one phosphate linkage is substituted for a vinylphosphonate group in the 4' position of the nucleoside sugar ring (3',3'-c-(2F,2'dAMP,2F,2'dA^{CH=CHP}), **4**; Fig. 2). The resulting CDNs were biophysically characterized for their ability to bind to STING, and the crystal structure of the best ligand bound to the STING protein was solved by X-ray crystallography. The biological activity was further validated in reporter cell-based assays and translated into cytokine production using a physiologically relevant cell system of peripheral blood mononuclear cells (PBMCs). Moreover, acyloxymethyl prodrugs of the lead CDNs were prepared, showing up to 1000-fold higher potency *in vitro* cell-based assays than their parent CDNs and the clinical candidate ADU-S100. To assess the therapeutic potential of these vinylphosphonate CDNs, the lead prodrug was validated for its anti-cancer efficacy in the 4T1 syngeneic mouse model of breast cancer.

2. Results and discussion

Naturally occurring CDNs (e.g., **1** and **2**) consist of adenosine and/or guanosine bound to phosphate groups connecting 2'-5' and 3'-5' or 3'-5' and 3'-5' hydroxy groups, respectively. In synthetic CDNs, various modifications have been introduced to purine nucleobases [31,32], sugar rings (e.g., 2'-deoxyribose, using carbasugars) [28,33] and phosphate linkers (e.g., phosphorothioate, phosphoramidate and boranophosphate) [34,35], in addition to substitutions of nucleobases for (hetero)aromates [19]. But as far as we know, no vinylphosphonate CDN has been reported thus far even though vinylphosphonate nucleotide units have been integrated into oligonucleotide strands targeting viral diseases as S-antigen transporting inhibitors [36]. In this study, we substituted one of the phosphate linkers for a rigid moiety – vinylphosphonate – to alter the macrocycle geometry and thus improve the CDN properties.

In previous studies, we had demonstrated that CDNs containing 2'-deoxy-2'-fluoro-modified nucleosidic units outperform CDNs with other functional groups on the sugar ring [20,31,37,38]. Accordingly, we started our synthesis from 2'-fluoro-2'-deoxynucleosides and from

simple 2'-deoxynucleosides. For brevity, the schemes and text only describe the synthesis of the lead CDN, **4**. Other CDNs were synthesized using similar procedures starting from different nucleosides. The synthetic experiments are described in detail in Supporting Information (SI).

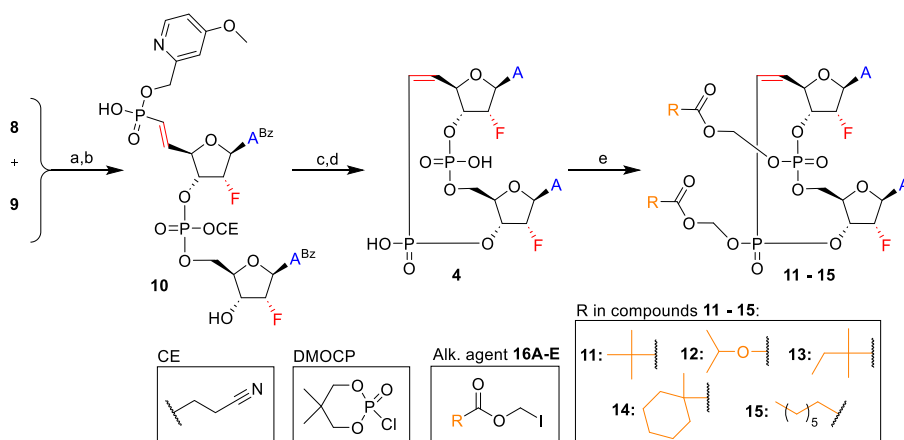
By Wittig-Horner-Emmons olefination, the vinylphosphonate group was attached to the 4' position of 2'-fluoro-2'-deoxyadenosine, yielding diethylphosphonate **7**. In turn, the phosphonate diester was transformed to 4-methoxy-pyridine-2-methyl monoester with a free 3' hydroxy group (**8**), affording a monomer appropriately protected for CDN cyclization (Scheme 1). Under phosphite triester synthesis conditions, the reverse phosphoramidite **9** was attached to the free 3' position, leading to a linear dinucleotide **10**. After macrocycle closure with 5,5-dimethyl-2-oxo-2-chloro-1,3,2-dioxaphosphinane (DMOCP), the 4-methoxy-pyridine-2-methyl and nucleobase protections were cleaved, yielding the final cyclic dinucleotide **4** (Scheme 2). This synthetic approach was inspired by a known oligonucleotide synthesis protocol [39] never before used in the synthesis of CDNs.

Using this method, we prepared a set of CDNs. These CDNs were then assessed for their ability to bind to the STING protein (Table 1) based on the STING-ligand complex stability using a previously described DSF assay [20,31]. The results showed that most of our molecules increased the melting temperature of wild-type (WT) and AQ STING haplotypes, some of which by a margin similar to that of canonical 3',3'cGAMP **2**, as outlined in Table 1.

Determining the *in vitro* STING agonistic potency of our CDNs required circumventing their poor cellular uptake as negatively charged molecules. For this reason, we performed a cell-based reporter assay including a mild detergent (digitonin A) for cell membrane permeabilization. Membrane permeabilization enabled us to easily measure STING activation by our CDNs in cells, without involving CDN transporters such as SLC19A1 [40] (Table 1). As expected, we found the highest agonistic potencies in CDNs with the 2'-fluorine modification [38].

Even removing one of the fluorine atoms increased the EC₅₀ values. However, this increase was lower when the other fluorine remained on the 4'-vinylphosphonate unit. The A-G combination of nucleobases provided the best results, whereas the A-A combination had similar potencies, except for the REF haplotype of STING, which showed the strongest increase. Most importantly, the two best compounds, **4** and **16**, displayed similar or better agonistic properties than the canonical **1** or **2** and the ADU-S100 **3**.

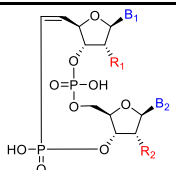
To delve into the CDN binding mode, we grew crystals of the STING/**4** complex, which diffracted to 2.3 Å resolution and belonged to the



Scheme 2. Typical example of the synthesis of 3',3'-c-(2F,2'dAMP,2F,2'dA^{CH=CHP}) **4** and its prodrugs **11–15**^a.

^aReagents and conditions: a) py-TFA, tBHP, ACN, r. t., 1 h; b) DCA, DCM, r. t., 10 min; c) DMOCP, py, r. t., 1 h then H₂O, 70 °C, 12 h; d) CH₃NH₂, r. t., 1 h, 24% over 4 steps; e) DOWEX 50(TBA+), "alkylating agent", r. t., 1 h, 49% for **11**.

Table 1
In vitro activity of the CDNs in the digitonin HEK 293T cell-based reporter assay.



B ₁	B ₂	R ₁	R ₂	DSF ΔT _m (°C) ^a (± SEM)		Digitonin HEK 293T cell-based reporter assay - EC ₅₀ (μM) ^b (±SEM)				
				WT	AQ	WT	HAQ	REF	AQ	Q
1 (2',3'-cGAMP)				15.3 (±0.17)	22.7 (±0.19)	0.02 (±0.004)	0.02 (±0.003)	0.07 (±0.02)	0.04 (±0.01)	0.05 (±0.02)
2 (3',3'-cGAMP)				5.1 (±0.14)	13.2 (±0.16)	0.12 (±0.03)	0.12 (±0.01)	4.26 (±0.49)	0.26 (±0.09)	2.06 (±0.36)
3 (ADU-S100)				9.3 (±0.18)	17.1 (±0.20)	0.08 (±0.01)	0.26 (±0.05)	1.64 (±0.28)	0.23 (±0.03)	1.01 (±0.19)
16	G	A	F	9.4 (±0.40)	15.2 (±0.60)	0.02 (±0.005)	0.06 (±0.02)	0.32 (±0.16)	0.08 (±0.02)	0.46 (±0.24)
4	A	A	F	6.0 (±0.92)	11.3 (±0.32)	0.03 (±0.02)	0.10 (±0.07)	11.95 (±3.55)	0.10 (±0.00)	1.05 (±0.05)
17	A	G	F	5.2 (±0.92)	11.4 (±0.17)	0.12 (±0.06)	0.14 (±0.08)	9.50 (±0.70)	0.13 (±0.06)	2.95 (±0.15)
18	A	A	F	2.7 (±0.20)	8.9 (±0.55)	0.28 (±0.01)	0.27 (±0.07)	>45	0.39 (±0.10)	1.5 (±1.00)
19	G	G	F	3.4 (±0.71)	8.8 (±1.72)	0.50 (±0.10)	0.95 (±0.25)	3.69 (±3.32)	0.95 (±0.05)	8.65 (±7.75)
20	A	G	H	4.8 (±0.03)	11.9 (±0.25)	0.70 (±0.00)	0.35 (±0.05)	25.50 (±1.50)	0.29 (±0.11)	4.15 (±0.65)
21	A	A	H	2.3 (±0.30)	8.2 (±0.40)	0.75 (±0.15)	0.28 (±0.09)	>45	0.4 (±0.00)	6.57 (±1.93)
22	G	A	H	1.9 (±0.30)	8.6 (±0.3)	0.78 (±0.16)	0.44 (±0.09)	>45	0.21 (±0.05)	>45
23	A	G	H	0.9 (±0.00)	4.5 (±0.14)	10.79 (±8.60)	0.24 (±0.15)	>45	0.39 (±0.14)	>45

^aThe values of the melting temperature (ΔT_m) assessed by differential scanning fluorimetry (DSF) with WT and AQ STING haplotypes; ΔT_m values are expressed as mean ± standard error of the mean (SEM) of at least two independent experiments. ^bResults from the digitonin assay using 293T reporter cells expressing different STING protein haplotypes; EC₅₀ values are expressed as mean ± SEM of at least two independent experiments measured in triplicates. The green frame highlights the most active compounds.

tetragonal P₄1₂2 space group. Subsequently, the structure was solved by molecular replacement and further refined to R_{work} = 23.1% and R_{free} = 25.8% and good geometry (Table S2). In line with the 2:1 protein:ligand stoichiometry of complexes formed by STING and CDNs, our STING/4 complex contained one molecule of STING per asymmetric unit and one molecule of compound 4 per two asymmetric units (Fig. 3A). Compound 4 was bound to STING through multiple interactions, including both direct (via Arg238) and indirect water-mediated hydrogen bonds (via Ser162, Arg232, Tyr240, Thr263, and Thr267) (Fig. 3B).

When comparing the structure of STING in the STING/4 complex with its previously published structure in a complex with 3',3'-c-di(2'F,2'dAMP) (pdb entry 6Z0Z [38]) by superposition, we found similar positions of adenine bases, sugar rings, including 2'-deoxy-2'-fluoro modifications, and the canonically linked phosphate group. Nevertheless, the macrocycle geometry was altered, showing a different orientation of the rigid vinylphosphonate group (Fig. 3C), albeit without significantly affecting the conformation of the ligand binding site of STING. Moreover, the rigidity of the vinylphosphonate group was compensated for by a conformational change of Ser162 and by a minor shift of a water molecule involved in an indirect water-mediated hydrogen bond between Ser162 and the phosphate/phosphonate

group of the ligand (Fig. 3D). Therefore, our results highlight the plasticity of the ligand binding site of STING, which is mainly mediated by several coordinated water molecules at the bottom of the ligand binding pocket of STING.

Optimizing our CDN design required improving the cellular uptake of the negatively charged CDNs to enhance their cellular potency. For this purpose, we followed a prodrug strategy. More specifically, we attached pivaloyloxymethyl (POM)-like groups successfully used in commercially available phosphonate-based antiviral drugs [41] to both phosphate and phosphonate groups. In other words, we masked the charge of CDN linkers, a strategy that had already proved successfully in our group [20,42].

The synthetic method was adapted also for this class of CDNs. In this reaction, a tetrabutylammonium salt of the parent CDN was mixed with a suitable acyloxymethyl iodide in acetonitrile, resulting in a mixture of three HPLC separable diastereomers at an approximately 1:1:5 ratio. Based on our previous findings [42], we concluded that the main and most lipophilic isomer bears both prodrug moieties, which are positioned below the plane of the macrocycle (further listed as isomer "C"). Furthermore, we determined that, in the minor isomers, the prodrug moieties are either in a trans configuration (inseparable mixture, listed as "B") or positioned above the plane (listed as "A"). Our NMR study

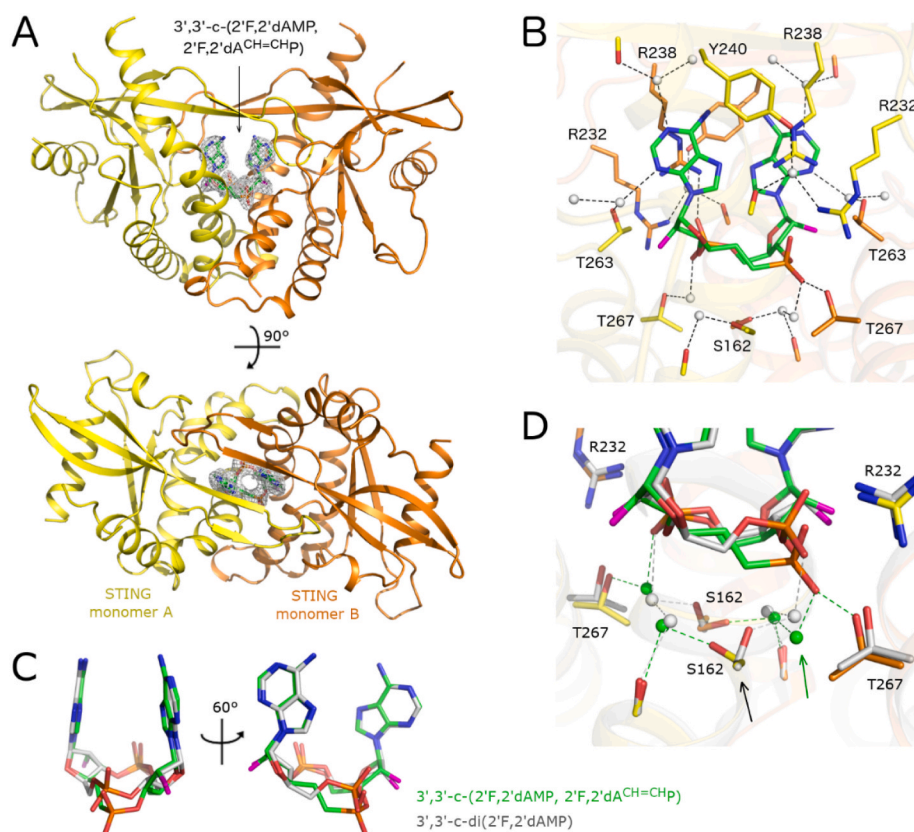


Fig. 3. Crystal structure of human STING in complex with **4**; **A** - Overall view of the STING/**4** complex; the protein backbone is shown in cartoon representation, and the two STING monomers are depicted in yellow and orange. Compound **4** is shown in stick representation according to the following elements and respective colors: carbon in green, nitrogen in blue, oxygen in red, phosphorus in orange, and fluorine in magenta. The *Fo*-*Fc* omit map contoured at 3σ is shown around the ligand. **B** - Detailed view of the ligand binding site; compound **4** and side chains of selected STING amino acid residues are shown in stick representation, and the carbon atoms are colored according to the protein/ligand assignment and other elements as in **A**. Water molecules are shown as grey spheres. Hydrogen atoms are not shown. Selected hydrogen bonds involved in the STING-**4** interaction are presented as dashed black lines. **C** - Superposition of $3',3'$ -*c*-($2F,2'dAMP,2F,2'dA^{CH=CHP}$) (**4**) and $3',3'$ -*di*($2F,2'dAMP$) (pdb entry 6Z0Z [38]) bound to STING. The ligands are shown in stick representation with carbon atoms colored in green (**4**) or grey ($3',3'$ -*di*($2F,2'dAMP$)) and other elements colored as in **A**. The STING protein molecules are not shown. **D** - Plasticity of the ligand binding site. Ligand **4** and $3',3'$ -*di*($2F,2'dAMP$) were superposed and depicted as in **C**. STING in a complex with **4** is depicted as in **B**, whereas STING in a complex with $3',3'$ -*di*($2F,2'dAMP$) is depicted with carbon atoms colored in grey. Water molecules and selected hydrogen bonds involved in STING-**4** and STING- $3',3'$ -*di*($2F,2'dAMP$) interactions are presented as green and grey spheres and dashed lines, respectively. The changed conformation of Ser162 and the position of a water molecule are indicated with black and green arrows, respectively.

combined with DFT calculations supported these conclusions (see supporting information).

In a proof-of-concept experiment, we synthesized a bis-POM prodrug of $3',3'$ -*c*-($2F,2'dAMP,2F,2'dA^{CH=CHP}$) **11**, which showed an excellent performance in the 293T cell-based reporter assay without membrane permeabilizing digitonin A. Moreover, the EC_{50} of compound **11** surpassed that of benchmark compounds **1** and **3** by 24 000 and 2400 fold, respectively (Table 2). Ultimately, we validated the choice of our lead CDN by comparing its bis-POM prodrug with the bis-POM of prodrug $3',3'$ -*c*-($2F,2'dAMP,2'dA^{CH=CHP}$) **24**, whose EC_{50} value was significantly higher.

We also explored four further types of promoieties ranging in polarity from the more polar isopropoxyloxycarbonyloxymethyl (POC) to the very lipophilic *n*-octyloxymethyl. In the standard assay using HEK 293T reporter cells, the most active prodrug was **15C**, which outperformed the parent CDN by over 11 000 fold and ADU-S100 by almost 5000 fold.

STING-dependent cytokine induction is responsible for amplifying and broadening the immune response to trigger antibacterial and antiviral host immune defense and specific antitumor immunity [15,37,43,44]. Thus, we assessed the cytokine induction effectiveness of our compounds in a biologically relevant system, using human peripheral blood mononuclear cells (PBMCs). In addition, because $IFN\alpha$, among other $IFNs$, is crucial for tumor-initiated T cell priming in mice [44], we also looked into cGAS-STING-dependent tumor necrosis factor alpha ($TNF\alpha$) and $IFN\gamma$ secretion, as early and late reactions to cGAS-STING activation [45]. To mimic *in vivo* clearance of our compounds, cells were pulsed with CDNs for only 1 h and washed before determining the level of cytokines after another 15 h of incubation.

As in the 293T cell-based reporter assays, even our CDN prodrugs were markedly more potent than their parent compounds and the benchmark molecules $2',3'$ cGAMP **1** and ADU-S100 **3** in this PBMC assay

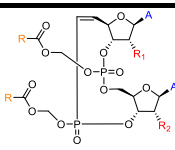


(Table 3). In fact, all POM-like prodrugs outperformed their parent compounds, with differences ranging from 380 to 7600 times. Considering these findings, we used the *in vitro* plasma stability of our prodrugs as a criterion to select the best promoiety for subsequent *in vivo* tests of our CDNs aimed at assessing their anticancer efficacy.

We feared that our prodrugs could be unstable *in vivo* because mouse plasma esterases, in particular, can quickly cleave promoieties before the intracellular uptake of active species, thereby preventing the practical use of candidate CDNs [46]. Even though our compounds were relatively stable in human plasma ($T_{1/2}$ 19–130 min), our promoieties were rapidly (<4 min) cleaved in carboxyesterase-rich mouse plasma. Nevertheless, compound **14C** was able to withstand the environment of mouse plasma, with a half-life of 21 min. Based on these results, we selected **14C** as the best candidate for assessing the therapeutic potential of a vinylphosphonate-based CDN *in vivo*, using the 4T1 syngeneic mouse model of breast cancer.

4T1 tumor-bearing mice (Fig. 4A) responded to intratumoral (IT) administration of both parent (**4**) and prodrug (**14C**) STING agonists in a dose-dependent manner (Fig. 4B). This post-treatment effect reached 80 and 70% tumor growth inhibition (TGI) in the groups treated with 2 and 0.67 mg/kg of prodrug **14C**, respectively (Fig. 4C), surpassing 60% TGI throughout the experiment. Although the difference between the two doses (2 and 0.67 mg/kg prodrug) was nonsignificant (Fig. 4B), at a dose of 2 mg/kg, the prodrug potently induced tumor regression in 7 of 8 mice, and only 1 mouse was completely non-respondent (Fig. 4D), possibly due to a poor T-cell dependent anti-tumor response (Fig. 4F). The lowest dose of prodrug **14C**, i.e., 0.22 mg/kg, and all doses of the parent molecule **4** showed a limited response. IT administration of **14C** enhanced TGI by eliciting a more robust tumor-specific T cell response than the parent molecule **4** (Fig. 4F and S5D).

The induction of tumor antigen-specific T cells, particularly the

Table 2
In vitro activity of the CDNs and prodrugs in a standard HEK 293T WT STING cell-based reporter assay.

			Standard HEK 293T cell-based reporter assay - EC ₅₀ (μM) ^a			
			30 min		7 h	
	R ₁	R ₂	EC ₅₀ (± SEM)	EC ₅₀ par/pro	EC ₅₀ (± SEM)	EC ₅₀ par/pro
1			233.00 (±34.79)		36.91 (±8.02)	
3			24.18 (±2.67)		3.32 (±0.43)	
4	F	F	50.14 (±16.87)		21.55 (±11.45)	
18	H	F	>200 (±0.00)		71.75 (±7.75)	
11A	F	F	0.13 (±0.02)	386	0.060 (±0.01)	359
11B	<i>t</i> Bu	F	0.030 (±0.01)	1 671	0.022 (±0.008)	980
11C	F	F	0.010 (±0.008)	5 014	0.012 (±0.009)	1 874
24A	H	F	9.93 (±1.53)	>20	12.10 (±0.40)	6
24B	<i>t</i> Bu	F	0.55 (±0.05)	>363	0.675 (±0.03)	106
24C	H	F	0.21 (±0.09)	>952	0.260 (±0.10)	276
12A	F	F	7.950 (±4.35)	6	9.500 (±8.10)	2
12B	<i>O</i> iPr	F	2.63 (±2.28)	19	1.25 (±1.15)	17
12C	F	F	0.25 (±0.05)	200	0.07 (±0.03)	308
13A	F	F	0.45 (±0.05)	111	0.15 (±0.05)	144
13B		F	0.035 (±0.005)	1 432	0.014 (±0.007)	1 596
13C	F	F	0.035 (±0.02)	1 432	0.007 (±0.003)	3 079
14A	F	F	0.500 (±0.10)	100	0.25 (±0.05)	86
14B		F	0.225 (±0.08)	223	0.080 (±0.02)	269
14C	F	F	0.030 (±0.006)	1 671	0.013 (±0.003)	1 616
15A	F	F	0.035 (±0.005)	1 432	0.020 (±0.000)	1 078
15B	C ₇	F	0.004 (±0.0006)	12 534	0.003 (±0.0005)	8 620
15C	F	F	0.005 (±0.0005)	11 141	0.003 (±0.001)	8 620

^aResults from the standard assay using HEK 293T reporter cells expressing the WT STING haplotype.

The cells were either incubated with compounds for 30 min, washed twice and incubated for another 6.5h or incubated continuously in the presence of the compounds for 7h. EC₅₀ values are expressed as mean ± standard error mean (SEM) of two or more independent experiments performed in triplicates; par – parent CDN, pro – prodrug; the green frame highlights the most active compounds.

AH1+ CD8 T cell subset, was also dose dependent. This response was the highest in the group of mice treated with 2 mg/kg prodrug, leading to effective tumor eradication (Fig. 4B–D). Mice treated with 2 mg/kg prodrug had significantly higher levels of the AH1-positive subset than mice treated with the vehicle (Fig. 4F). The potency of the parent and prodrug molecules displayed an efficacy trend of 2 mg/kg prodrug >> 0.67 mg/kg prodrug >0.22 mg/kg prodrug ~6, 2 and 0.67 mg/kg parent in inducing a systemic tumor-specific immune response. The induced activity was ten times higher in the prodrug group than in the vehicle-treated group. By contrast, activity was only four times higher in the parent group than in the vehicle-treated group.

The tumor burden gradually decreased without systemic toxicity as none of the tested STING agonist treatments affected the mice, neither their physiology, as shown by weight change (Fig. 4E), nor their survival (Figure S5A,B). All parent/prodrug doses were well tolerated. The maximum weight loss was 3%, on D7 after IT administration of 6 mg/kg parent CDN (Fig. 4E). A few animals in the study had to be prematurely sacrificed due to tumor rupture on D15 in the group treated with 0.67 mg/kg parent CDN and to the tumor size limit on D19 for mice in the parent- (6, 2, 0.67 mg/kg) and prodrug-administered (2, 0.22 mg/kg) groups (Figure S5A,B,C).

The *in vivo* anti-tumor activity of compound **14C** reported above matches that of the most potent compounds currently known [19,28], which are 2',3'-CDNs with phosphorothioate linkages. Our observations also corroborate previous findings [47], which provided strong evidence

that 3',3' CDNs act as competent anti-cancer agents in various cancers (e. g., colon and lung cancer). Other studies have previously demonstrated [19,28] that the STING pathway-dependent activation of innate immunity induces the expression of stimulatory markers on human DCs *in vitro* and type I IFN and pro-inflammatory cytokine secretion *in vivo*. Furthermore, our results suggest that tumor eradication by **14C** is modulated by systemic immune activation.

Our lead CDN is also more potent than the most prominent CDN-based STING agonists despite the lower dose [15,28] and fewer IT administrations [48]. Furthermore, the activity of compound **14C** may be higher in humans than in mice because **14C** is more stable in human plasma than in mouse plasma. Overall, our results build on previous findings [15,19,28,48], which have also demonstrated enhanced tumor shrinkage following IT administration of modified STING agonists using *in vivo* syngeneic colon, melanoma, hepatocellular, breast mouse cancer models, thus highlighting CDNs as potent cancer therapeutic targets. Considering the properties of the vinylphosphonate CDNs discussed above, these compounds are suitable preclinical candidates for cancer therapy. In their ongoing development, we aim at further boosting their efficacy by administering them with suitable immunotherapy antibodies, using them as antibody-drug conjugates (ADCs) and assessing their activity *in vivo* alongside checkpoint inhibitors. This research may open up opportunities for developing immunotherapy approaches based on IT administration of vinylphosphonate CDNs for terminally ill cancer patients.

Table 3
In vitro activity evaluation of prodrugs in a peripheral blood mononuclear cells (PBMC) assay.

Compound	Chemical structure	PBMC assay/cytokine production - EC ₅₀ (μM) ^a			Plasma stability T _{1/2} (min)	
		IFN γ	TNF α	IFN α	Human	Mouse
1 (2',3'-cGAMP)		50 (±17)	216 (±64)	93 (±38)		
3 (ADU-S100)		140 (±10)	150 (±21)	50 (±17)		
4		36	76	110		
11B		0.75 (±0.40)	0.33 (±0.10)	0.35 (±0.07)		
11C		0.05 (±0.01)	0.04 (±0.01)	0.06 (±0.01)	49	4
12C		1.30 (±0.30)	0.25 (±0.05)	0.60 (±0.40)		
13C		0.02 (±0.01)	0.12 (±0.03)	0.06 (±0.03)	86	4
14B		0.25 (±0.3)	0.14 (±0.09)	0.3 (±0.10)		
14C		0.07 (±0.03)	0.06 (±0.05)	0.11 (±0.04)	130	21
15B		0.06 (±0.02)	0.07 (±0.03)	0.08 (±0.02)		
15C		0.17 (±0.04)	0.28 (±0.07)	0.12 (±0.04)	19	3

^aPeripheral blood mononuclear cells (PBMC) isolated from the buffy coats of healthy donors were pulsed with compounds for 60 minutes, washed twice and incubated for another 15 hours. EC₅₀ values are expressed as mean values ± standard error mean (SEM) of at least two independent experiments measured in triplicates. The green frame highlights the compounds selected for further evaluation.

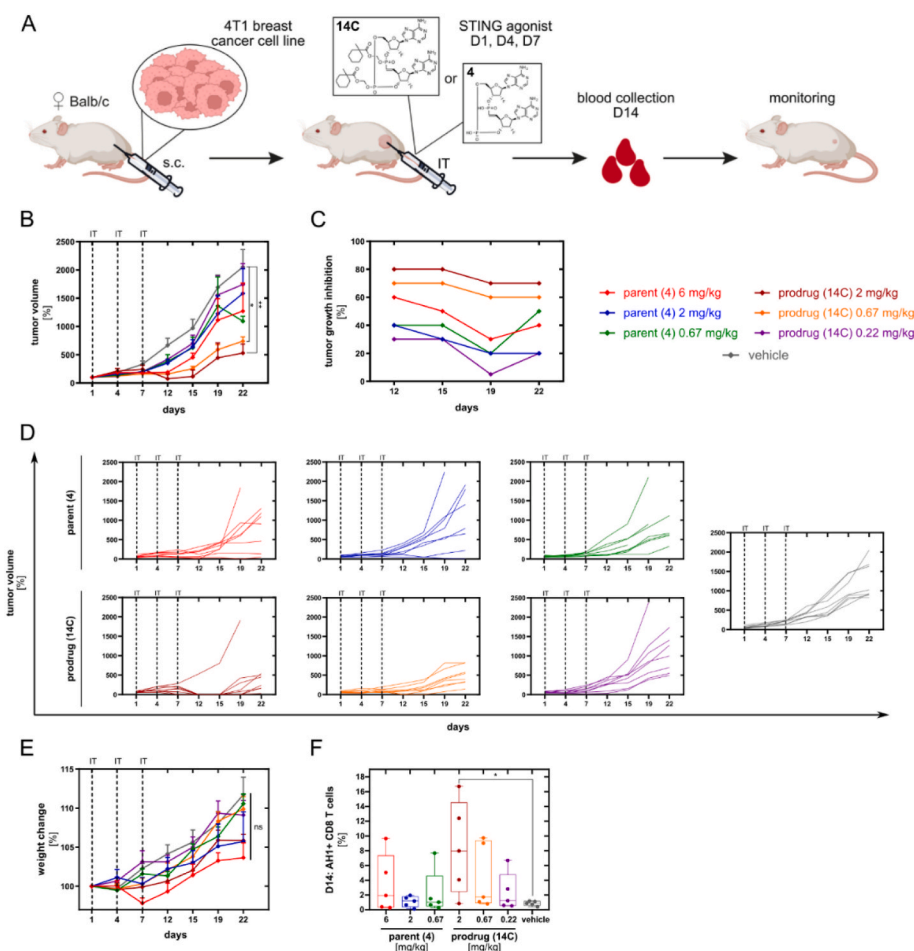


Fig. 4. STING pathway intratumorally activated by the STING agonist modulates a potent anti-cancer immune response. **A** - Flowchart of the experiment created with BioRender.com. Mice bearing s. c. 4T1 tumor in a single flank (right side) were IT administered with either vehicle or test compounds, 4 and 14C, at 6, 2, 0.67 mg/kg parent CDN 4 and 2, 0.67, 0.22 mg/kg prodrug 14C, on day 1, 4, and 7 (D1, D4, and D7; dotted lines), respectively, monitoring tumor-specific AH1+ CD8 T cell response in blood seven days after the third injection (D14). **B** - Tumor volume expressed as percentage of the mean tumor volume at day 1. The mean end-point tumor volume of each experimental group was compared with that of the vehicle group by Kruskal-Wallis one-way analysis of variance (ANOVA) with *post hoc* Dunn's test for multiple comparisons. Treatments with doses of 2 and 0.67 mg/kg significantly differed from the treatment with vehicle $**p = 0.0015$, and $*p = 0.0268$, respectively. **C** - TGI in the post-treatment period. **D** - Tumor volume curves of the individual groups. **E** - Weight change expressed as percentage of the mean weight at day 1, stratified by groups. The mean end-point weight of each experimental group was compared with that of the vehicle by Kruskal-Wallis ANOVA, showing no significant difference. **F** - Tumor specific AH1+ CD8 T cell response; using the one-tailed Mann-Whitney *U* test, the groups were compared with the vehicle. The dose of 2 mg/kg 14C significantly differed from the dose of the vehicle ($*p = 0.0278$); $*p < 0.05$, $**p < 0.01$; ns = non-significant; 8 mice per test group.

3. Conclusion

Vinylphosphonate CDNs act as potent STING agonists. Based on their biophysical and biological activity in vitro cell-based assays, POM-like prodrugs display excellent cellular uptake and STING agonistic properties, outperforming canonical CDNs and the clinical candidate ADU-S100 **3** and showing EC₅₀ values 3–4 orders of magnitude lower than these benchmarks. *In vivo*, IT administration of **14C** reduces tumor volume in a mouse model of breast cancer, thus demonstrating the pre-clinical potential of **14C** as a highly promising activator of the cGAS-STING signaling pathway. Ultimately, in the tumor microenvironment, **14C** harnesses the host immune system to eradicate tumors by eliciting an innate and specific adaptive immune response.

4. Experimental section

Unless stated otherwise, all solvents were evaporated at 40 °C at 2 kPa, and the compounds were dried at 30 °C at 2 kPa. Starting compounds and reagents were purchased from commercial suppliers (Sigma-Aldrich, Fluorochem, Acros Organics, Carbosynth) and used without further purification. Acetonitrile was dried using activated 3A molecular sieves. Analytical Thin-Layer Chromatography (TLC) was performed on silica gel-precoated aluminum plates with a fluorescent indicator (Merck 60 F254). Column chromatography (both normal and reverse phase) was performed on a 40–60 µm silica gel using an ISCO flash chromatography system. Purity of the final compounds was determined by UPLC MS and was 95% or higher.

Analytical High-Performance Liquid Chromatography (HPLC), mass spectra, UV absorbance and compound purity were measured on a Waters Ultra-high Performance Liquid Chromatography-Mass Spectrometry (UPLC-MS) system consisting of a Waters UPLC H-Class Core System, a UPLC photodiode array (PDA) detector and a Waters SQD2 or QDa mass spectrometer. The MS method used was electrospray ionization (ESI)⁺ and/or ESI⁻, cone voltage = 15 V, mass detector range 200–1000 Da or 200–1250 Da. Two sets of HPLC conditions were used as indicated: (a) C18 (column: Waters Acquity UPLC BEH C18 column, 1.7 mm, 2.1 × 100 mm; LC method: H₂O/CH₃CN, 0.1% formic acid as a modifier, gradient 0–100%, run length 7 min, flow 0.5 ml/min) and (b) HILIC (column: SeQuant ZIC-pHILIC, 5 µm, polymeric, 50 × 2.1 mm; LC method: CH₃CN/0.01 M aqueous ammonium acetate gradient 10–60%, run length 7 min, flow 0.3 ml/min).

The final products (CDNs and CDN prodrugs) were purified by semipreparative HPLC (Luna, 5 µm, C18 250 × 21 mm or 150 × 10 mm). The free CDNs were prepared using triethylammonium bicarbonate (TEAB) as a modifier. TEAB was removed from the collected fractions by 3 cycles of co-evaporation with methanol. The concentrations of CDNs and the respective prodrugs were measured using an Implen Nano-Photometer N60 Touch system. The purity of all compounds was higher than 95% unless stated otherwise.

CAUTION! The CDN prodrugs (**11–15**, **24**) are highly biologically active molecules with very high lipophilicity. We expect good skin and cell permeability and possible systemic reaction on inhalation of lyophilizate or on skin contact with a prodrug solution in organic solvents (ACN and DMSO). We recommend that adequate safety precautions be taken in the preparation of these compounds.

NMR spectra were recorded on Bruker Avance III HD machines (¹H at 400, 500 or 600 MHz) using a solvent signal as a reference. *Tert*-butyl alcohol was used as an internal standard in D₂O solutions. Chemical shifts (δ) and coupling constants (*J*) were expressed in ppm and Hz, respectively. All structures were confirmed, and ¹H and ¹³C signals were assigned by combining 1D and 2D NMR (H,H-COSY, H,C-HSQC, H,C-HMBC) techniques and using standard pulse programs from the library of the spectrometer; gradient selection was used in the 2D experiments. Mass spectra were measured on an LTQ Orbitrap XL using electrospray ionization (ESI).

N-(9-((2*R*,3*R*,4*R*,5*R*)-4-(bis(4-methoxyphenyl)(phenyl)methoxy)-3-

fluoro-5-(hydroxymethyl) tetrahydrofuran-2-yl)-9*H*-purin-6-yl)benzamide (**6**).

Commercially available **5** (Carbosynth Ltd., 12 g, 32 mmol) was azeotroped with pyridine (2x 50 mL), dissolved in pyridine (130 mL) and TBDMSCl (4.85 g, 32 mmol) was added in one portion. The reaction mixture was then stirred for another 5 h, a further portion of TBDMSCl (9.7 g, 64 mmol) was subsequently added, and the reaction mixture was stirred for 12 h. Excess TBDMSCl was quenched with MeOH (50 mL), and all volatiles were evaporated. The resulting sticky syrup was azeotroped with pyridine (2x 20 mL), dissolved in pyridine (150 mL) and DMTrCl (22 g, 64 mmol) was added in one portion. The reaction mixture was stirred at 60 °C for 24 h and then quenched with methanol, and all volatiles were evaporated. The resulting crude, protected nucleoside was azeotroped with toluene (3x 100 mL) and dissolved in THF (150 mL) and TBAF (1 M in THF, 96 mL) was added in one portion. The reaction mixture was then stirred at room temperature for 12 h. All volatiles were evaporated; subsequently, FCC on a silica gel (acetone in cyclohexane, 10–100%) afforded **6** (16.2 g, 75% over 3 steps).

Diethyl ((*E*)-2-((2*R*,3*R*,4*R*,5*R*)-5-(6-benzamido-9*H*-purin-9-yl)-3-(bis(4-methoxyphenyl)(phenyl) methoxy)-4-fluorotetrahydrofuran-2-yl) vinyl)phosphonate (**7**).

6 (5 g, 7.4 mmol) was azeotroped with dimethylformamide (DMF; 2x 30 mL) and dissolved in anhydrous DMF (50 mL). Dimethyl sulfoxide (DMSO; 3.2 mL, 44.4 mmol) and 1-ethyl-3-(3-dimethylaminopropyl) carbodiimide (EDC HCl; 4.3 g, 22.2 mmol) were added followed by a dropwise addition of a solution of pyridine (0.6 mL, 7.4 mmol) and trifluoroacetic acid (TFA; 0.3 mL, 3.7 mmol) in DMF (25 mL). The reaction mixture was stirred at room temperature for 2 h, diluted with ethyl acetate (500 mL) and washed with saturated aqueous NaHCO₃ solution (250 mL) and brine (250 mL). The organic layer was dried with sodium sulfate and evaporated. The residue was azeotroped with toluene (3x 100 mL) and used in the following reaction without further purification. LCMS analysis showed a single product: [598]⁺ (hydrate).

Under argon, *n*BuLi (1.6 M in hexanes, 4.6 mL) was added dropwise to a –78 °C solution of tetraethyl methylenediphosphonate (2.8 mL, 11.1 mmol) in anhydrous THF (50 mL). The reaction mixture was stirred at –78 °C for 15 min. A solution of the crude aldehyde in anhydrous THF (50 mL) was added dropwise, and the reaction mixture was stirred at –78 °C for 15 min. LCMS analysis showed approximately 75% conversion, which remained unchanged in the next 15 min. The reaction was quenched by adding 50 mL of saturated aqueous NH₄Cl solution. The residue was diluted with ethyl acetate (500 mL) and washed with water (100 mL) and brine (100 mL). The organic phase was dried with sodium sulfate and evaporated. Flash chromatography (acetone in cyclohexane, 20–60%) afforded **7** (3.3 g, 55%). Electrospray ionization high-resolution mass spectrometry (ESI HRMS) (C₄₃H₄₄FN₅O₈P) calculated: 808.8236; found: 808.8241; ¹H NMR (401 MHz, DMSO-*d*₆) δ 11.23 (s, 1H, NH), 8.63 (s, 1H, H-2), 8.51 (s, 1H, H-8), 8.06–7.99 (m, 2H, Bz-*o*), 7.68–7.61 (m, 1H, Bz-*p*), 7.58–7.48 (m, 4H, Bz-*m*, DMTr-*o*), 7.42–7.36 (m, 4H, DMTr-2), 7.36–7.29 (m, 1H, DMTr-*m*), 7.29–7.21 (m, 1H, DMTr-*p*), 6.94–6.83 (m, 4H, DMTr-3), 6.51 (dd, *J*_{5',*p*} = 21.2, *J*_{5',*6'*} = 16.9, *J*_{5',*4'*} = 6.7 Hz, 1H, H-5'), 6.35 (dd, *J*_{1',*F*} = 20.5, *J*_{1',*2'*} = 1.6 Hz, 1H, H-1'), 6.17 (dd, *J*_{6',*p*} = 20.1, *J*_{6',*5'*} = 17.2 Hz, 1H, H-6'), 4.88 (dd, *J*_{3',*F*} = 19.4, *J*_{3',*2'*} = 7.8, *J*_{3',*2'*} = 4.3 Hz, 1H, H-3'), 4.70 (t, *J*_{4',*3'*} = *J*_{4',*5'*} = 7.3 Hz, 1H, H-4'), 4.16 (dd, *J*_{2',*F*} = 51.2, *J*_{2',*3'*} = 3.2 Hz, 1H, H-2'), 4.00–3.85 (m, 4H, Et-CH₂), 3.71 and 3.69 (s, 3H, DMTr-OCH₃), 1.19 and 1.17 (t, *J*_{CH₃,CH₂} = 7.1 Hz, 6H, Et-CH₃). ¹³C NMR (101 MHz, DMSO-*d*₆) δ 165.78 (CON), 158.64 (DMTr-4), 151.73 (C-2), 151.18 (C-4), 150.77 (C-6), 146.71 (d, *J*_{5',*p*} = 5.5 Hz, C-5'), 145.02 (DMTr-*i*), 144.07 (C-8), 135.41 and 135.37 (DMTr-1), 133.40 (Bz-*i*), 132.72 (Bz-*p*), 130.45 and 130.40 (DMTr-2), 128.68 (Bz-*o*,*m*), 128.08 (DMTr-*o*,*m*), 127.27 (DMTr-*p*), 125.95 (C-5), 122.10 (d, *J*_{6',*p*} = 182.6 Hz, C-6'), 113.48 and 113.42 (DMTr-3), 91.91 (d, *J*_{2',*F*} = 188.2 Hz, C-2'), 87.30 (d, *J*_{1',*F*} = 35.6 Hz, C-1'), 87.07 (DMTr-C), 81.46 (d, *J*_{4',*p*} = 23.6 Hz, C-4'), 75.01 (d, *J*_{3',*F*} = 15.0 Hz, C-3'), 61.59 and 61.57 (d, *J*_{CH₂,*p*} = 5.7 Hz, Et-CH₂), 55.22 (DMTr-OCH₃), 16.38 and 16.34 (d, *J*_{CH₃,*p*} = 5.7 Hz, Et-CH₃). ³¹P NMR (162 MHz, DMSO-*d*₆) δ

18.76. ^{19}F NMR (377 MHz, DMSO- d_6) δ -195.11 (dt, J = 51.0, 19.9 Hz).

(4-Methoxypyridin-2-yl)methyl hydrogen ((*E*)-2-((2*R*,3*R*,4*R*,5*R*)-5-(6-benzamido-9*H*-purin-9-yl)-4-fluoro-3-hydroxytetrahydrofuran-2-yl)vinyl)phosphonate (**8**).

TMSBr (2.6 mL, 20 mmol) was added to a solution of **7** (2 g, 2.5 mmol) in pyridine (25 mL), and the reaction mixture was stirred at room temperature for 12 h. Volatiles were evaporated, the residue was dissolved in chloroform (150 mL), washed with 0.2 M TEAB (3x 30 mL), dried with sodium sulfate and evaporated to dryness. This crude free phosphonate was combined with 4-methoxypyridine *N*-oxide hydrate (1.1 g, 7.4 mmol), azeotroped with pyridine (2x 10 mL) and dissolved in pyridine (20 mL). (4-Methoxy-pyridin-2-yl)-methanol (1.04 mg, 0.75 mmol) was added followed by DMOCP (1.37 mg, 7.4 mmol), and the reaction mixture was stirred at ambient temperature for 1 h. The reaction was quenched by adding water (10 mL), and the resulting mixture was heated to 70 °C for 48 h. All volatiles were evaporated forming a crude phosphonate monoester with the DMT protection cleaved. RP FCC (ACN in water 0–50%) afforded 850 mg (60% over 2 steps) of **8**: HRMS ESI ($\text{C}_{25}\text{H}_{25}\text{FN}_6\text{O}_7\text{P}$) calculated: 571.4816; found: 571.4808; ^{13}C NMR (101 MHz, DMSO- d_6) δ 166.14 (Pic-4), 165.81 (CON), 160.89 (d, $J_{2,\text{P}}$ = 7.5 Hz, Pic-2), 152.01 (C-2), 151.80 (C-4), 150.74 (C-6), 149.88 (Pic-6), 143.59 (C-8), 140.06 (C-5'), 133.52 (Bz-*i*), 132.66 (Bz-*p*), 128.71 and 128.66 (Bz-*o*, Bz-*m*), 128.56 (d, $J_{6,\text{P}}$ = 171.3 Hz, C-6'), 125.96 (C-5), 108.81 (Pic-5), 106.70 (Pic-3), 93.58 (d, $J_{2,\text{F}}$ = 185.9 Hz, C-2), 85.59 (d, $J_{1,\text{F}}$ = 34.7 Hz, C-1'), 82.85 (d, $J_{4,\text{P}}$ = 21.1 Hz, C-4'), 72.80 (d, $J_{3,\text{F}}$ = 16.0 Hz, C-3'), 65.95 (d, $J_{\text{CH}_2,\text{P}}$ = 4.5 Hz, Pic-CH₂), 55.39 (OCH₃). ^1H NMR (401 MHz, DMSO- d_6) δ 11.24 (s, 1H, NH), 8.73 (s, 1H, H-2), 8.63 (s, 1H, H-8), 8.26 (d, $J_{6,5}$ = 5.7 Hz, 1H, Pic-6), 8.08–8.02 (m, 2H, Bz-*o*), 7.68–7.61 (m, 1H, Bz-*p*), 7.58–7.52 (m, 2H, Bz-*m*), 7.01 (d, $J_{3,5}$ = 2.6 Hz, 1H, Pic-3), 6.81 (dd, $J_{5,6}$ = 5.8, $J_{5,3}$ = 2.6 Hz, 1H, Pic-5), 6.42 (dd, $J_{5,\text{P}}$ = 19.1, $J_{5,6'}$ = 16.9, $J_{5,4'}$ = 6.3 Hz, 1H, H-5'), 6.38 (dd, $J_{1,\text{F}}$ = 20.5, $J_{1,2'}$ = 1.6 Hz, 1H, H-1'), 5.99 (t, $J_{6,5'}$ = $J_{6,\text{P}}$ = 16.5 Hz, 1H, H-6'), 5.57 (dd, $J_{2,\text{F}}$ = 52.4, $J_{2,3'}$ = 4.7, $J_{2,1'}$ = 1.8 Hz, 1H, H-2'), 4.72 (d, $J_{\text{CH}_2,\text{P}}$ = 7.5 Hz, 2H, Pic-CH₂), 4.65 (dd, $J_{3,\text{F}}$ = 22.1, $J_{3,4'}$ = 8.1, $J_{3,2'}$ = 4.7 Hz, 1H, H-3'), 4.42 (bt, $J_{4,3'}$ = $J_{4,5'}$ = 7.2 Hz, 1H, H-4'), 3.78 (s, 3H, OCH₃). ^{31}P NMR (162 MHz, DMSO- d_6) δ 11.26. ^{19}F NMR (377 MHz, DMSO- d_6) δ -200.74 (dt, $J_{\text{F},2'}$ = 52.6, $J_{\text{F},3'}$ = $J_{\text{F},1'}$ = 21.2 Hz).

((2*R*,3*R*,4*R*,5*R*)-5-(6-benzamido-9*H*-purin-9-yl)-3-(bis(4-methoxyphenyl)(phenyl)methoxy)-4-fluorotetrahydrofuran-2-yl)methyl (2-cyanoethyl) diisopropylphosphoramidite (**9**).

Through a syringe, 2-Cyanoethyl *N,N,N,N'*-tetraisopropylphosphorodiamidite (3.6 mL, 11.8 mmol), followed by tetrazole (0.45 M in ACN, 33 mL) were sequentially added to a solution of **6** (4 g, 5.9 mmol) in 1,2-dichloroethane (DCE; 40 mL) under argon atmosphere. The reaction mixture was stirred at room temperature for 30 min, diluted with DCM (300 mL), washed with sat. Aq. NaHCO₃ (100 mL), dried over sodium sulfate and evaporated. The crude product was dissolved in DCM (10 mL) and applied to a preconditioned silicagel column (10% acetone in cyclohexane, 1% triethylamine (TEA)) and eluted with a gradient of acetone in cyclohexane 10–50%. The product was freeze-dried from benzene to afford **9** (4.57 g, 88%) as a mixture of diastereomers. ^{31}P NMR (162 MHz, Benzene- d_6) δ 151.69, 151.66. ^{19}F NMR (377 MHz, Benzene- d_6) δ -198.55 (dt, J = 51.2, 17.7 Hz), -198.96 (dd, J = 51.1, 21.6, 15.6 Hz).

(2*R*,3*R*,3*aR*,7*aR*,9*R*,10*R*,10*aR*,14*aR*,*E*)-2,9-Bis(6-amino-9*H*-purin-9-yl)-3,10-difluoro-5,12-dihydroxy-3,3*a*,7,7*a*,9,10,10*a*,14*a*-octahydro-2*H*-difuro[2,3-*e*:2',3'-*k*][1,3,7]trioxo[2,8]diphosphacyclododecine 5,12-dioxide (**4**).

A mixture of **8** (250 mg, 0.44 mmol) and pyridinium trifluoroacetate (127 mg, 0.66 mmol) was azeotroped with dry ACN (3 x 10 mL), suspended in dry ACN (10 mL) and stirred overnight in a sealed vessel over activated 3 Å molecular sieves. In a separate flask, **9** (480 mg, 0.55 mmol) was codistilled with dry ACN (3 x 10 mL), dissolved in dry ACN (5 mL) and stirred overnight in a sealed vessel over activated 3 Å molecular sieves. Through a syringe, a solution of **9** was transferred to the flask with the suspension of **8** with py-TFA, and the resulting solution

was stirred for 1 h at room temperature. tert-Butyl hydroperoxide (TBHP; 5.5 M solution in decane, 239 μL , 1.32 mmol) was added, and the reaction mixture was stirred for another 30 min. The reaction mixture was quenched with NaHSO₃ (39% in water, 316 μL , 1.18 mmol) and evaporated to afford crude tritylated linear dimer, which was used in the next reaction without further purification.

To a solution of this residue in DCM (20 mL), water (79 μL , 4.38 mmol) and then a solution of DCA (509 μL , 3.9 mmol) in DCM (10 mL) were added dropwise. After a stirring period of for 30 min, the reaction mixture was quenched by adding pyridine (5 mL). All solids were removed by filtration and thoroughly washed with pyridine. Volatiles were evaporated, and the linear dimer was isolated by reversed phase flash column chromatography (RP FCC; acetonitrile (ACN) in 0.05 M NH₄COOH, 0–100%) as a mixture of diastereomers.

Subsequently, the linear dimer was azeotroped with pyridine (2x 10 mL) and dissolved in pyridine (10 mL), DMOCP (283 mg, 1.53 mmol) was added, and the reaction mixture was stirred at room temperature for 1 h. Water (4 mL) was added, and the reaction mixture was stirred at 60 °C for 12 h to cleave the phosphonate ester group. During this reaction, the cyanoethyl protection was partly cleaved as well. All volatiles were evaporated, and the residue was treated with methylamine (33% ethanolic solution, 10 mL) for 1 h. The deprotected cyclic dinucleotide was purified on semipreparative HPLC (ACN in 0.1 M TEAB, 0–30%). Appropriate fractions were pooled, evaporated, codistilled with methanol (5 x 20 mL), dissolved in water (1 mL) and slowly passed through a 3 mL column of Dowex 50 (Na⁺ cycle). Freeze-drying the eluent afforded the sodium salt of **4** (70 mg, 24%). HPLC retention time (HILIC, min): 4.02. ^1H NMR (501 MHz, D₂O) δ 8.40 (s, 1H, A1-8), 8.16 (s, 1H, A2-8), 8.11 (s, 1H, A1-2), 8.07 (s, 1H, A2-2), 6.69 (dd, $J_{5,\text{P}}$ = 19.6, $J_{5,6'}$ = 17.0, $J_{5,4'}$ = 8.2 Hz, 1H, A2-5'), 6.39 (d, $J_{1,\text{F}}$ = 16.5 Hz, 1H, A1-1'), 6.36 (dd, $J_{1,\text{F}}$ = 19.4, $J_{1,2'}$ = 0.8 Hz, 1H, A2-1'), 6.24 (td, $J_{6,5'}$ = $J_{6,\text{P}}$ = 17.0, $J_{6,4'}$ = 1.0 Hz, 1H, A2-6'), 5.61 (dd, $J_{2,\text{F}}$ = 52.0, $J_{2,3'}$ = 4.6, $J_{2,1'}$ = 0.8 Hz, 1H, A2-2'), 5.45 (dd, $J_{2,\text{F}}$ = 51.6, $J_{2,3'}$ = 4.2 Hz, 1H, A1-2'), 5.01 (ddd, $J_{3,\text{F}}$ = 23.0, $J_{3,\text{P}}$ = 10.4, $J_{3,4'}$ = 9.2, $J_{3,2'}$ = 4.6 Hz, 1H, A2-3'), 4.80 (m, 2H, A1-3', A2-4'), 4.45 (m, 2H, A1-4', A1-5'a), 4.04 (dd, J_{GEM} = 11.0, $J_{5,\text{b},4'}$ = 2.5 Hz, 1H, A1-5'b). ^{31}P NMR (202 MHz, D₂O) δ 13.76, -0.60. ^{19}F NMR (470 MHz, DMSO- d_6) δ -196.80, -197.47.

{[(1*R*,6*R*,9*R*,10*S*,15*R*,17*R*,18*R*)-9,17-Bis(6-amino-9*H*-purin-9-yl)-12-[[[2,2-dimethylpropanoyl]oxy]methoxy]-18-fluoro-3,12-dioxo-2,4,7,11,13,16-hexaoxa-3 λ^5 ,12 λ^5 -diphosphatricyclo[13.3.0.0 6 ,1 9]octadecan-3-yl]oxy]methyl 2,2-dimethylpropanoate (**11**).

Na⁺ or TEA⁺ cation was exchanged for a tetrabutylammonium by slowly passing an aqueous solution of CDN through a DOWEX 50 column (TBA⁺ cycle, 1 mL of resin per 2 μmol of CDN). All volatiles were evaporated subsequently. **4** (25 mg, 22 μmol , TBA⁺) as azeotroped with dry toluene (2 x 5 mL) and dry ACN (2 x 5 mL), dissolved in dry ACN (5 mL) and treated with iodomethyl pivalate (53 mg, 220 μmol) under argon atmosphere at room temperature for 4 h while monitoring its progress by LCMS. Full conversion to dialkylated products failed: at one point, overreacted products were formed faster than monoalkylated CDN was consumed. The reaction mixture was quenched with 2 mL of water, most of the acetonitrile was evaporated, and the residue was purified on semi-preparative HPLC affording **11A-C** (separate diastereomers, HPLC ratio ca 1:1:5). **11A**, 1.4 mg (7%); HPLC retention time (C18, min): 3.31. **11B**, 1.0 mg (5%); HPLC retention time (C18, min): 3.45. **11C**, 7.1 mg (37%); HPLC retention time (C18, min): 3.64. ^1H NMR (501 MHz, CD₃CN) δ 8.22 (s, 1H) and 8.02 (s, 2H) and 7.92 (s, 1H, A-2, B-2, A-8, B-8), 6.23 (dd, $J_{1,\text{F}}$ = 20.3, $J_{1,2'}$ = 1.2 Hz, 1H, A-1'), 6.05 and 6.04 (bs, 2H, NH₂), 5.49–5.77 (m, 7H, A-2', A-3', B-3', O-CH₂-O), 5.35 (m, 1H, B-2'), 4.17–4.49 (m, 8H, B-1', B-4', B-5', A-4', A-5'), 1.23 and 1.15 (s, 9H, CH₃). ^{31}P NMR (202.4 MHz, CD₃CN) δ -2.15 (s), -2.42 (s). ^{19}F NMR (470.4 MHz, CD₃CN) δ -195.73 (dt, $J_{\text{F},2'}$ = 51.9, $J_{\text{F},1'}$ = $J_{\text{F},3'}$ = 19.9 Hz).

4.1. Differential scanning fluorimetry (DSF)

The stability of protein-ligand complex was examined by the DSF method as previously described [20,49]. Briefly, the DSF was run in 96-well optical plates (LightCycler® 480 Multiwell Plate 96 white, Roche). STING protein WT and AQ allelic forms were used. Thermal denaturation of samples was performed on a LightCycler 480 Instrument II (Roche). The first derivative of fluorescence intensity referring to thermal denaturation of the protein was determined as melting temperatures (T_m), and the thermal shift (ΔT_m) was calculated as the difference of T_m of ligand-free and protein in complex with CDN [19,49].

4.2. In vitro cell-based activity of CDNs

The activity of tested CDNs was determined using reporter HEK 293T ISRE cell lines expressing various STING protein haplotypes in digitonin (R232 (WT), R293Q (Q), R232H (REF), G230A-R293Q (AQ), R71H-G230A-R293Q (HAQ) allelic forms) and standard (WT allelic form) reporter assays as previously described [31, 42].

Digitonin reporter assay: 293T reporter cells stably expressing different STING protein haplotypes were seeded into poly(*D*-lysine)-coated 96 (white) plates. The next day, the cells were treated with serial dilutions of compounds in digitonin buffer. After 30 min incubation, the digitonin buffer was removed, cells were washed, and fresh medium was added for the following incubation time of 5h. The luminescence was assessed using Bright-Glo Luciferase Assay System reagent measured on Spark (TECAN, Grödig, Austria). GraphPad Prism (La Jolla, USA) was used to calculate the 50% effective concentration (EC_{50}).

Standard reporter assay: The 293T reporter cells stably expressing WT STING protein haplotype were seeded into poly(*D*-lysine)-coated 96 (white) plates. The next day, the cells were treated with serially diluted compounds in a cell culture medium. The cells were incubated for 30 min, washed and incubated for a further 6.5h or incubated for a complete period of 7h. After the incubation time, cells were washed and incubated for an additional 6.5h, or the complete 7h, the luminescence was measured using Bright-Glo Luciferase Assay System reagent and the EC_{50} values were calculated.

All incubations were performed at standard conditions (37 °C, 5% CO_2 atmosphere).

4.3. Activity of CDNs in PBMC assay

Buffy coats from healthy individuals, who signed an informed consent form, were obtained from the Institute of Hematology and Blood Transfusion (IHBT, Prague, Czech Republic). The study was approved by the institutional review board of IHBT, under evidence number June 13, 2012. Peripheral blood mononuclear cells (PBMC) were isolated from buffy coats using SepMate™-50 (Stem Cell Technologies), by Ficoll® Paque Plus (GE Healthcare) density gradient centrifugation, according to the manufacturer's protocol, and treated as previously described [31, 42]. The cells were incubated with compounds for 60 min, then were washed twice and further incubated for the following 15 h. The levels of human $IFN\alpha$, $IFN\gamma$ and $TNF\alpha$ secreted into the cell culture medium were determined in ProcartaPlex™ assays (Invitrogen; ThermoFisher Scientific) using a Magpix Luminex Instrument (Merck), according to the manufacturer's instruction. Compound-relevant EC_{50} values were calculated using GraphPad Prism (La Jolla) [31,42].

4.4. In vitro plasma stability assay

The *in vitro* plasma stability of compounds was evaluated with midazolam as an internal standard and propantheline as a positive control. Stability was assessed in both human (cat# S4180-100, VWR) and mouse (cat# S2162-100, VWR) plasma. Prodrugs were pre-diluted in DMSO and transferred into the plasma pre-heated to 37 °C. This mixture of prodrugs (5 μ M final concentration) and plasma was then

continuously incubated at 37 °C, and at each time point (0, 2, 4, 8, 16, 30, 120 min), the aliquot was collected and mixed with a solution of acetonitrile/1 μ M midazolam in ratio 1:3. All timepoint samples were tempered at –80 °C for 30 min to precipitate the proteins and spun down at 6000×g for 20 min at –20 °C. The supernatant was then mixed with deionized water in a ratio of 2.5:1 towards analysis. For analysis, the ACQUITY UPLC®H-Class PLUS System was used with an MS SQ Detector 2 (Waters, USA) with an ACQUITY UPLC BEH C18 1.7 μ m 2.1 × 50 mm column (Waters, USA). The column was pre-heated to 40 °C. The mobile phase – a gradient of 10 mM ammonium acetate to acetonitrile in 4 min – was used at a flow rate of 0.5 ml/min. The data were acquired and processed in MassLynx (Waters, USA) and TargetLynx (Waters, USA).

4.5. In vivo mouse syngeneic model of breast cancer

All animal procedures were approved by the Institutional Ethical Committee, Academic Animal Care Committee and in line with national guidelines, ensuring the welfare of experimental animals (ev. nb. 09/2020, 89/2020, Czech Republic). Female adult BALB/c mice were purchased from Charles River Laboratory and housed in specific pathogen-free conditions in an individually ventilated cage system with access to food and water *ad libitum*. All mice were housed under controlled temperature and light settings.

The 4T1 mouse breast cancer cell line was purchased from ATCC (ATCC® CRL-2539™). Cells were cultivated and maintained in a humidified incubator (5% CO_2 atmosphere) at 37 °C in RPMI-1640 Medium (Biowest) supplemented with 10% (v/v) heat-inactivated fetal bovine serum (FBS, Capricorn Scientific) and 1% (v/v) penicillin-streptomycin (P/S, Biowest).

A single flank tumor model was initiated by subcutaneously (s.c.) implanting 50,000 4T1 cells in 100 μ L of PBS mixed with matrigel (Corning® Matrigel® Basement Membrane Matrix, Corning) at a 1:1 ratio into the right flank of each test animal. Tumor size was measured in two dimensions, twice a week, using a digital caliper. Tumor volume was calculated according to the formula: tumor volume [mm^3] = (length × width [2])/2. Once they reached the target range of 60–70 mm^3 tumor volume, the mice were randomized into treatment and control groups.

4.6. In vivo immunotherapy

Mice randomized based on tumor volume (mean value of 65 mm^3 , described above) were intratumorally (IT) treated with the lead compounds, parent (4) and prodrug (14C). Therapeutic agents were freshly diluted on each day of administration to yield dosing to the designed concentration in a volume of 20 μ L. The compounds were dissolved in the tempered formulation buffers (10% ethanol, 40% PEG300 (Sigma-Aldrich) in Hank's Balanced Salt Solution (HBSS, Sigma Aldrich, cat#H6648). Towards IT administration, mice were anesthetized with inhalation anesthesia. The tumors were IT treated with 6, 2, 0.67 mg/kg of parent CDN (4) and 2, 0.67, 0.22 mg/kg of prodrug (14C) three times, on D1, D4 and D7, respectively. The mice were monitored on daily basis for overt signs of any adverse, treatment-related side effect, and were weighed twice a week. Notes were taken for each individual mouse. Seven days after the third IT injection (experimental D14), blood was collected into heparin microvette tubes (Microvette CB 500, Sarstedt) and centrifuged for 3000×g, 5 min at RT. Blood immune cells were immunophenotyped for tumor specific immune response (see below). The mean percentage of tumor growth inhibition (%TGI) was calculated post treatment using the following equation: TGI [%] = ((mean tumor volume of control vehicle group – mean tumor volume of treated group) × 100).

4.7. Tumor-specific immune response

Tumor-specific immune response was determined by

immunophenotyping based on flow cytometry (FC) approach. Blood immune cells were collected, and red blood cells were lysed using red blood cell lysis buffer (0.1 mM EDTA (Sigma-Aldrich), 12 mM NaHCO₃ (Penta), 155 mM NH₄Cl (Sigma-Aldrich); sterile filtered (0.45 μm, Sigma-Aldrich)) for 5 min at RT. Immune cells were immunophenotyped as previously described [45,50] using viability dye (Zombie NIR™ Fixable Viability Kit, BioLegend), monoclonal antibodies: BUV395 hamster anti-mouse CD3e, BV605 rat anti-mouse CD4, V450 rat anti-mouse CD8a (all BD Biosciences). Specific staining using MHC I dextramer: PE labelled AH1 peptide (SPSYVYHQF, Immudex) was performed according to the manufacturer's instructions. Specific and control samples of unstained cells, positive control for dead cells (cells in PBS incubated for 5 min at 65 °C and further stained with a live/dead marker), and fluorescence minus one (FMO) and isotype controls (ISO) were prepared. Samples were measured immediately without a fixation step in a single tube format in 250 μL of Flow cytometry buffer (FC buffer, PBS containing 5% FBS) using a BD LSRFortessa flow cytometer (BD Biosciences). Data were acquired using FACS Diva software (version 8.0.1, BD Biosciences). Debris were excluded by forward and side scatter gating followed by doublet and dead cell exclusion. Populations of interest were gated by exclusion of non-desired cells and by specific selection as follows: AH1+ CD8⁺ CD3⁺ T cells. The data were analyzed using FlowJo software (version 10, BD Biosciences). Individual populations and their subsets were quantified as a frequency (%) of cells in a superior parent population.

4.8. Statistical analysis

GraphPad Prism (La Jolla, CA) version 8.0.1 was used to analyze all experimental data. All data are expressed as means ± standard error mean (SEM). Relative tumor volume and mouse weight were both normalized to D1-related. The normality of distributions was tested using the Shapiro-Wilk test. Mann-Whitney *U* test was used to analyze differences in AH1 CD8 T cell cytotoxic response. The endpoint (D22) values of tumor volume and mouse weight, and then individual times to endpoints, were analyzed using Kruskal-Wallis; si significantly different data (*p* < 0.05), were analyzed by post hoc Dunn's multiple comparisons. The survival of mice was compared with Logrank test. No animals or related samples were excluded from the analysis. Significance levels were set as following: nonsignificant (ns) at *p* > 0.5, significant at **p* < 0.05, ***p* < 0.01.

5. PDB ID codes

The PDB code for human WT STING with bound compound 4 is 7Q85. Authors will release the atomic coordinates and experimental data upon publication of the article.

Declaration of competing interest

The authors declare the following financial interests/personal relationships which may be considered as potential competing interests: A patent application (WO2022007986) was filed with the results from this study. European patent (EP3936514) was granted in May 2023. This study was partly funded by Gilead Sciences, Inc.

Data availability

Data will be made available on request.

Acknowledgments

This work was supported by National Institute of Virology and Bacteriology (Programme EXCELES, ID Project No. LX22NPO5103) - Funded by the European Union - Next Generation EU, by the Ministry of Health of the Czech Republic (grant NU20-05-00472), by the Czech

Academy of Sciences (RVO: 61388963), and by Gilead Sciences, Inc. For the *in vivo* experiments, the authors used the services of the Czech Centre for Phenogenomics at the Institute of Molecular Genetics supported by the Czech Academy of Sciences RVO 68378050 and by project LM2018126 of the Czech Centre for Phenogenomics, also funded by the Ministry of Education, Youth and Sports of the Czech Republic. Accordingly, the authors are grateful to the Czech Centre for Phenogenomics, Institute of Molecular Genetics of the Czech Academy of Sciences, for conducting the *in vivo* experiments. The authors also thank to Dr. Lenka Vaneková for her help with the manuscript figures and to Dr. Carlos V. Melo for editing the manuscript.

Appendix A. Supplementary data

Supplementary data to this article can be found online at <https://doi.org/10.1016/j.ejmech.2023.115685>.

Abbreviations used

CDN	cyclic dinucleotide
GMP	guanosine monophosphate
AMP	adenosine monophosphate
cGAS	cyclic GMP-AMP synthase
STING	stimulator of interferon genes
ICB	immune-checkpoint blockade
CTLA-4	cytotoxic T-lymphocyte antigen 4
PD-1	programmed cell death protein 1
TBK1	TANK-Binding Kinase 1
IRF3	interferon regulatory factor 3
IFN	interferon
PBMC	peripheral blood mononuclear cells
ACN	acetonitrile
TBDMS	tert-butyldimethylsilyl
EDCI	1-Ethyl-3-(3-dimethylaminopropyl)carbodiimide
DMOCP	2-Chloro-5,5-dimethyl-1,3,2-dioxaphosphorinane 2-oxide
CE	cyanoethyl
DCA	dichloroacetic acid
DSF	differential scanning fluorimetry
POM	pivaloyloxymethyl
IT	intratumoral
TGI	tumor growth inhibition
ADC	antibody-drug conjugate

References

- [1] T. Ugai, N. Sasamoto, H.Y. Lee, M. Ando, M. Song, R.M. Tamimi, I. Kawachi, P. T. Campbell, E.L. Giovannucci, E. Weiderpass, T.R. Rebbeck, S. Ogino, Is early-onset cancer an emerging global epidemic? Current evidence and future implications, *Nat. Rev. Clin. Oncol.* 19 (10) (2022) 656–673.
- [2] R.L. Siegel, K.D. Miller, H.E. Fuchs, A. Jemal, *Cancer statistics, 2022*, *CA Cancer J Clin* 72 (1) (2022) 7–33.
- [3] J.A. Wargo, A. Reuben, Z.A. Cooper, K.S. Oh, R.J. Sullivan, Immune effects of chemotherapy, radiation, and targeted therapy and opportunities for combination with immunotherapy, *Semin. Oncol.* 42 (4) (2015) 601–616.
- [4] K. Baksh, J. Weber, Immune checkpoint protein inhibition for cancer: preclinical justification for CTLA-4 and PD-1 blockade and new combinations, *Semin. Oncol.* 42 (3) (2015) 363–377.
- [5] S. Li, Y. Simoni, S. Zhuang, A. Gabel, S. Ma, J. Chee, L. Islas, A. Cessna, J. Creaney, R.K. Bradley, A. Redwood, B.W. Robinson, E.W. Newell, Characterization of neoantigen-specific T cells in cancer resistant to immune checkpoint therapies, *Proc. Natl. Acad. Sci. U. S. A.* 118 (30) (2021).
- [6] G. Berger, E.H. Knelson, J.L. Jimenez-Macias, M.O. Nowicki, S. Han, E. Panagioti, P.H. Lizotte, K. Adu-Berchie, A. Stafford, N. Dimitrakakis, L. Zhou, E.A. Chioocca, D. J. Mooney, D.A. Barbie, S.E. Lawler, STING activation promotes robust immune response and NK cell-mediated tumor regression in glioblastoma models, *Proc. Natl. Acad. Sci. U. S. A.* 119 (28) (2022), e2111003119.
- [7] F. Mpekris, C. Voutouri, J.W. Baish, D.G. Duda, L.L. Munn, T. Stylianopoulos, R. K. Jain, Combining microenvironment normalization strategies to improve cancer immunotherapy, *Proc. Natl. Acad. Sci. U. S. A.* 117 (7) (2020) 3728–3737.
- [8] R.T. Zur, G. Adler, K. Shamalov, Y. Tal, C. Ankrí, C.J. Cohen, Adoptive T-cell immunotherapy: perfecting self-defenses, *Experientia Suppl.* 113 (2022) 253–294.

- [9] P.A. Ott, F.S. Hodi, H.L. Kaufman, J.M. Wigginton, J.D. Wolchok, Combination immunotherapy: a road map, *J Immunother Cancer* 5 (2017) 16.
- [10] L. Ou, A. Zhang, Y. Cheng, Y. Chen, The cGAS-STING pathway: a promising immunotherapy target, *Front. Immunol.* 12 (2021), 795048.
- [11] E.R. Verrier, C. Langevin, Cyclic guanosine monophosphate-adenosine monophosphate synthase (cGAS), a multifaceted platform of intracellular DNA sensing, *Front. Immunol.* 12 (2021), 637399.
- [12] K.P. Hopfner, V. Hornung, Molecular mechanisms and cellular functions of cGAS-STING signalling, *Nat. Rev. Mol. Cell Biol.* 21 (9) (2020) 501–521.
- [13] S.R. Woo, M.B. Furtos, L. Corrales, S. Spranger, M.J. Furdyn, M.Y. Leung, R. Duggan, Y. Wang, G.N. Barber, K.A. Fitzgerald, M.L. Alegre, T.F. Gajewski, STING-dependent cytosolic DNA sensing mediates innate immune recognition of immunogenic tumors, *Immunity* 41 (5) (2014) 830–842.
- [14] Y. Zhu, X. An, X. Zhang, Y. Qiao, T. Zheng, X. Li, STING: a master regulator in the cancer-immunity cycle, *Mol. Cancer* 18 (1) (2019) 152.
- [15] K.E. Sivick, A.L. Desbrier, L.H. Glickman, G.L. Reiner, L. Corrales, N.H. Surh, T. E. Hudson, U.T. Vu, B.J. Francica, T. Banda, G.E. Katibah, D.B. Kanne, J.J. Leong, K. Metchette, J.R. Brumli, C.O. Ndubaku, J.M. McKenna, Y. Feng, L. Zheng, S. L. Bender, C.Y. Cho, M.L. Leong, A. van Elsas, T.W. Dubensky Jr., S.M. McWhirter, Magnitude of therapeutic STING activation determines CD8(+) T cell-mediated anti-tumor immunity, *Cell Rep.* 25 (11) (2018) 3074–3085 e5.
- [16] P. Gao, M. Ascano, Y. Wu, W. Barchet, B.L. Gaffney, T. Zillinger, A.A. Serganov, Y. Liu, R.A. Jones, G. Hartmann, T. Tuschl, D.J. Patel, Cyclic [G(2',5')ppA(3',5')p] is the meta-azo second messenger produced by DNA-activated cyclic GMP-AMP synthase, *Cell* 153 (5) (2013) 1094–1107.
- [17] D. Kalia, G. Merey, S. Nakayama, Y. Zheng, J. Zhou, Y. Luo, M. Guo, B.T. Roemke, H.O. Sintim, Nucleotide, c-di-GMP, c-di-AMP, cGMP, cAMP, (p)ppGpp signaling in bacteria and implications in pathogenesis, *Chem. Soc. Rev.* 42 (1) (2013) 305–341.
- [18] X. Sun, X. Yu, Y. Zhao, L. Xing, L. Na, Z. Chen, Z. Xiao, H. Dai, J. Yu, S. Long, Q. Wang, X. Shi, Z. Guan, M. Lei, Z. Yang, Cyclic diguanylate analogues: facile synthesis, STING binding mode and anti-tumor immunity delivered by cytidinyl/cationic lipid, *Eur. J. Med. Chem.* 247 (2023), 115053.
- [19] S. Vyskocil, D. Cardin, J. Ciavarrri, J. Conlon, C. Cullis, D. England, R. Gershman, K. Gigstad, K. Gipson, A. Gould, P. Greenspan, R. Griffin, N. Gulavita, S. Harrison, Z. Hu, Y. Hu, A. Hata, J. Huang, S.C. Huang, D. Janowick, M. Jones, V. Kolev, S. P. Langston, H.M. Lee, G. Li, D. Lok, L. Ma, D. Mai, J. Malley, A. Matsuda, H. Mizutani, M. Mizutani, N. Molchanova, E. Nunes, S. Pusalkar, C. Renou, S. Rowland, Y. Sato, M. Shaw, L. Shen, Z. Shi, R. Skene, F. Soucy, S. Stroud, H. Xu, T. Xu, A.O. Abu-Yousif, J. Zhang, Identification of novel carbocyclic pyrimidine cyclic dinucleotide STING agonists for antitumor immunotherapy using systemic intravenous route, *J. Med. Chem.* 64 (10) (2021) 6902–6923.
- [20] M. Dejmeek, M. Sala, A. Brazdova, L. Vanekova, M. Smola, M. Klima, P. Brehova, M. Budesinsky, M. Dracinsky, E. Prochazkova, M. Zavrel, O. Simak, O. Pav, E. Boura, G. Birkus, R. Nencka, Discovery of isonucleotidic CDNs as potent STING agonists with immunomodulatory potential, *Structure* 30 (8) (2022) 1146–1156 e11.
- [21] T.W. Dubensky Jr., D.B. Kanne, M.L.L. Leong, E.E. Lemmens, L.H. Glickman, Compositions Comprising Cyclic Purine Dinucleotides Having Defined Stereochemistries and Methods for Their Preparation and Use, 2014, WO2014093936.
- [22] J.M. Ramanjulu, G.S. Pesiridis, J. Yang, N. Concha, R. Singhaus, S.Y. Zhang, J. L. Tran, P. Moore, S. Lehmann, H.C. Eberl, M. Muelbauer, J.L. Schneck, J. Clemens, M. Adam, J. Mehlmann, J. Romano, A. Morales, J. Kang, L. Leister, T.L. Graybill, A. K. Charnley, G. Ye, N. Nevins, K. Behnia, A.I. Wolf, V. Kasparcova, K. Nurse, L. Wang, A.C. Puhl, Y. Li, M. Klein, C.B. Hopson, J. Guss, M. Bantscheff, G. Bergamini, M.A. Reilly, Y. Lian, K.J. Duffy, J. Adams, K.P. Foley, P.J. Gough, R. W. Marquis, J. Smothers, A. Hoos, J. Bertin, Design of amidobenzimidazole STING receptor agonists with systemic activity, *Nature* 564 (7736) (2018) 439–443.
- [23] J.M. Weiss, M.V. Guerin, F. Regnier, G. Renault, I. Galy-Fauroux, L. Vimeux, V. Feuillet, E. Peranzoni, M. Thoreau, A. Trautmann, N. Bercovici, The STING agonist DMXAA triggers a cooperation between T lymphocytes and myeloid cells that leads to tumor regression, *Oncology* 6 (10) (2017), e1346765.
- [24] S. Iurescia, D. Fioretti, M. Rinaldi, Targeting cytosolic nucleic acid-sensing pathways for cancer immunotherapies, *Front. Immunol.* 9 (2018) 711.
- [25] L. Wang, I. Shureiqi, J.R. Stroehlein, D. Wei, Novel and emerging innate immune therapeutic targets for pancreatic cancer, *Expert Opin. Ther. Targets* 22 (12) (2018) 977–981.
- [26] L. Corrales, L.H. Glickman, S.M. McWhirter, D.B. Kanne, K.E. Sivick, G.E. Katibah, S.R. Woo, E. Lemmens, T. Banda, J.J. Leong, K. Metchette, T.W. Dubensky Jr., T. F. Gajewski, Direct activation of STING in the tumor microenvironment leads to potent and systemic tumor regression and immunity, *Cell Rep.* 11 (7) (2015) 1018–1030.
- [27] F. Meric-Bernstam, R.F. Sweis, F.S. Hodi, W.A. Messersmith, R.H.I. Andtbacka, M. Ingham, N. Lewis, X. Chen, M. Pelletier, X. Chen, J. Wu, S.M. McWhirter, T. Muller, N. Nair, J.J. Luke, Phase I dose-escalation trial of MIW815 (ADU-S100), an intratumoral STING agonist, in patients with advanced/metastatic solid tumors or lymphomas, *Clin. Cancer Res.* 28 (4) (2022) 677–688.
- [28] W. Chang, M.D. Altman, C.A. Lesburg, S.A. Perera, J.A. Piesvaux, G.K. Schroeder, D.F. Wyss, S. Cemerski, Y. Chen, E. DiNunzio, A.M. Haidle, T. Ho, I. Kariv, I. Knemeyer, J.E. Kopinja, B.M. Lacey, J. Laskey, J. Lim, B.J. Long, Y. Ma, M. L. Maddess, B.S. Pan, J.P. Presland, E. Spooner, D. Steinhuebel, Q. Truong, Z. Zhang, J. Fu, G.H. Addona, A.B. Northrup, E. Parmee, J.R. Tata, D.J. Bennett, J. N. Cumming, T. Siu, B.W. Trotter, Discovery of MK-1454: a potent cyclic dinucleotide stimulator of interferon genes agonist for the treatment of cancer, *J. Med. Chem.* 65 (7) (2022) 5675–5689.
- [29] D.S. Kim, A. Endo, F.G. Fang, K.C. Huang, X. Bao, H.W. Choi, U. Majumder, Y. Y. Shen, S. Mathieu, X. Zhu, K. Sanders, T. Noland, M.H. Hao, Y. Chen, J.Y. Wang, S. Yasui, K. TenDyke, J. Wu, C. Ingersoll, K.A. Loiacono, J.E. Hutz, N. Sarwar, E7766, a macrocycle-bridged stimulator of interferon genes (STING) agonist with potent pan-genotypic activity, *ChemMedChem* 16 (11) (2021) 1740–1743.
- [30] F. Meric-Bernstam, R.F. Sweis, S. Kasper, O. Hamid, S. Bhatia, R. Dummer, A. Stradella, G.V. Long, A. Spreafico, T. Shimizu, N. Steeghs, J.J. Luke, S. M. McWhirter, T. Muller, N. Nair, N. Lewis, X. Chen, A. Beaur, L. Kattenhorn, M. Pelletier, S. Sandhu, Combination of the STING agonist MIW815 (ADU-S100) and PD-1 inhibitor spartalizumab in advanced/metastatic solid tumors or lymphomas: an open-label, multicenter, phase Ib study, *Clin. Cancer Res.* 29 (1) (2023) 110–121.
- [31] B. Novotna, L. Vanekova, M. Zavrel, M. Budesinsky, M. Dejmeek, M. Smola, O. Gutten, Z.A. Tehrani, M. Pimkova Polidarova, A. Brazdova, R. Liboska, I. Stepanek, Z. Vavrina, T. Jandusik, R. Nencka, L. Rulisek, E. Boura, J. Brynda, O. Pav, G. Birkus, Enzymatic preparation of 2'-5',3'-5'-cyclic dinucleotides, their binding properties to stimulator of interferon genes adaptor protein, and structure/activity correlations, *J. Med. Chem.* 62 (23) (2019) 10676–10690.
- [32] Z. Vavrina, P. Perlikova, N. Milisavljevic, F. Chevrier, M. Smola, J. Smith, M. Dejmeek, V. Havlicek, M. Budesinsky, R. Liboska, L. Vanekova, J. Brynda, E. Boura, P. Rezacova, M. Hocek, G. Birkus, Design, synthesis, and biochemical and biological evaluation of novel 7-deazapurine cyclic dinucleotide analogues as STING receptor agonists, *J. Med. Chem.* 65 (20) (2022) 14082–14103.
- [33] K. Biggadike, A.C. Champigny, D.M. Coe, D. Needham, D.T. Tape, Cyclic Dinucleotides as Modulators of STING, *Oct 22 2019*, p. 19. US 10450341.
- [34] G.C. Bignani, P. Connolly, J.P. Edwards, S. Emanuel, S. Laquerre, L. Tianbao, M. Richter, L. Beigelman, S.K. Thatikonda, G. Wang, M. Zhong, Cyclic Dinucleotides as Sting Agonists. WO2018098203 (A1), 2018/05/31/, 2018.
- [35] S. Emanuel, M. Richter, P.J. Connolly, J.P. Edwards, G. Wang, S.K. Thatikonda, L. Beigelman, M. Zhong, G. Bignani, W. Schepens, M. VIELLEVOYE, J.W.J.F. Thuring, CYCLIC DINUCLEOTIDES AS STING AGONISTS. WO2018/138685, 2018.
- [36] L. Beigelman, R. Pandey, V.K. Rajwanshi, D.B. Smith, L.M. Blatt, J. Hong, S-antigen Transport Inhibiting Oligonucleotide Polymers and Methods, 2020. WO2020097342 (A1), 2020/05/14/.
- [37] B. Novotna, L. Hala, M. Stas, O. Gutten, M. Smola, M. Zavrel, Z. Vavrina, M. Budesinsky, R. Liboska, F. Chevrier, J. Dobias, E. Boura, L. Rulisek, G. Birkus, Enzymatic synthesis of 3'-5', 3'-5' cyclic dinucleotides, their binding properties to the stimulator of interferon genes adaptor protein, and structure/activity correlations, *Biochemistry* 60 (48) (2021) 3714–3727.
- [38] M. Smola, O. Gutten, M. Dejmeek, M. Kozisek, T. Evangelidis, Z.A. Tehrani, B. Novotna, R. Nencka, G. Birkus, L. Rulisek, E. Boura, Ligand strain and its conformational complexity is a major factor in the binding of cyclic dinucleotides to STING protein, *Angew Chem. Int. Ed. Engl.* 60 (18) (2021) 10172–10178.
- [39] O. Pav, I. Kosiova, I. Barvik, R. Pohl, M. Budesinsky, I. Rosenberg, Synthesis of oligoribonucleotides with phosphonate-modified linkages, *Org. Biomol. Chem.* 9 (17) (2011) 6120–6126.
- [40] R.D. Luteijn, S.A. Zaver, B.G. Gowen, S.K. Wyman, N.E. Garelis, L. Onia, S. M. McWhirter, G.E. Katibah, J.E. Corn, J.J. Woodward, D.H. Raulet, SLC19A1 transports immunoreactive cyclic dinucleotides, *Nature* 573 (7774) (2019) 434–438.
- [41] K.M. Heidel, C.S. Dowd, Phosphonate prodrugs: an overview and recent advances, *Future Med. Chem.* 11 (13) (2019) 1625–1643.
- [42] M. Pimkova Polidarova, P. Brehova, M.M. Kaiser, M. Smola, M. Dracinsky, J. Smith, A. Marek, M. Dejmeek, M. Sala, O. Gutten, L. Rulisek, B. Novotna, A. Brazdova, Z. Janeba, R. Nencka, E. Boura, O. Pav, G. Birkus, Synthesis and biological evaluation of phosphoester and phosphorothioate prodrugs of STING agonist 3',3'-c-Di(2',2'dAMP), *J. Med. Chem.* 64 (11) (2021) 7596–7616.
- [43] G.N. Barber, STING: infection, inflammation and cancer, *Nat. Rev. Immunol.* 15 (12) (2015) 760–770.
- [44] M.S. Diamond, M. Kinder, H. Matsushita, M. Mashayekhi, G.P. Dunn, J. M. Archambault, H. Lee, C.D. Arthur, J.M. White, U. Kalinke, K.M. Murphy, R. D. Schreiber, Type I interferon is selectively required by dendritic cells for immune rejection of tumors, *J. Exp. Med.* 208 (10) (2011) 1989–2003.
- [45] M. Pimkova Polidarova, P. Brehova, M. Dejmeek, G. Birkus, A. Brazdova, STING agonist-mediated cytokine secretion is accompanied by monocyte apoptosis, *ACS Infect. Dis.* 8 (3) (2022) 463–471.
- [46] F.G. Bahar, K. Ohura, T. Ogihara, T. Imai, Species difference of esterase expression and hydrolase activity in plasma, *J. Pharmaceut. Sci.* 101 (10) (2012) 3979–3988.
- [47] L.T. Khoo, L.Y. Chen, Role of the cGAS-STING pathway in cancer development and oncotherapeutic approaches, *EMBO Rep.* 19 (12) (2018).
- [48] S. Stazzoni, D.F.R. Bohmer, F. Hernichel, D. Ozdemir, A. Pappa, D. Drexler, S. Bauernfried, G. Witte, M. Wagner, S. Veth, K.P. Hopfner, V. Hornung, L. M. Konig, T. Carell, Novel poxin stable cGAMP-derivatives are remarkable STING agonists, *Angew Chem. Int. Ed. Engl.* 61 (40) (2022), e202207175.
- [49] Z. Vavrina, O. Gutten, M. Smola, M. Zavrel, Z. Aliakbar Tehrani, V. Charvat, M. Kozisek, E. Boura, G. Birkus, L. Rulisek, Protein-ligand interactions in the STING binding site probed by rationally designed single-point mutations: experiment and theory, *Biochemistry* 60 (8) (2021) 607–620.
- [50] L. Vanekova, M.P. Polidarova, V. Veverka, G. Birkus, A. Brazdova, Multiparametric flow cytometry-based immunophenotyping of mouse liver immune cells, *Methods Protoc* 5 (5) (2022) 70.